Multistage single point incremental forming.

Silva, M. Beatriz; Skjødt, Martin; Bay, Niels; Martins, Paulo A.F.

Published in:
Proceedings of the Congress on Numerical Methods in Engineering

Publication date:
2011

Document Version
Publisher's PDF, also known as Version of record

Congress on Numerical Methods in Engineering 2011
Coimbra, 14 to 17 June, 2011

MULTISTAGE SINGLE POINT INCREMENTAL FORMING

M. Beatriz Silva[1], Martin Skjoedt[2], Niels Bay[2] and Paulo A. F. Martins[1]

1: IDMEC
Instituto Superior Técnico
Universidade Técnica de Lisboa
Av. Rovisco Pais, 1049-001 Lisboa, Portugal
e-mail: beatriz.silva@ist.utl.pt, pmartins@ist.utl.pt web: http://www.ist.utl.pt

2: Department of Mechanical Engineering
University Technical University of Denmark
DTU - Building 425, DK-2800, Kgs. Lyngby, Denmark
e-mail: mask@mek.dtu.dk, nbay@mek.dtu.dk web: http://www.me.mek.dtu.dk

Keywords: Single Point Incremental Forming, Experimentation, Finite Element Method

Abstract *Multistage SPIF is a state-of-the-art manufacturing process that allows small quantity production of complex sheet parts. This paper starts with the application of multistage SPIF with the objective of producing cylindrical cups with vertical walls. The strategy consists in forming a conical part with a taper angle in the first stage, followed by three subsequent stages that progressively change the conical towards the desired cylindrical geometry.*

The investigation includes material characterization, determination of forming limit curves (FLC) and fracture forming limit curves (FFLC), numerical simulation and experimentation. The assessment of numerical simulation with experimentation shows a good agreement between computed and measured strains and strain paths.

The results also reveal that the sequence of multistage forming has a large effect on the location of strain points in the principal strain space. Strain paths are linear in the first stage and highly non-linear in the subsequent forming stages.

The overall investigation show that the experimentally determined FFLC can successfully be employed to establish the forming limits of multistage SPIF and the last part of the paper includes three different industrial applications that were manufactured by the authors using metallic and polymeric materials.

1. INTRODUCTION

Single-point incremental forming (SPIF) is a new sheet-metal-forming process with a high-potential economic pay-off for rapid prototyping applications and for small-quantity production.

The basic components in the SPIF process are presented in Figure 1: sheet metal blank, blank holder, backing plate, and rotating single-point forming tool. The blank holder is utilized to clamp and hold the blank sheet in position during the SPIF process. The backing plate supports the sheet, and its opening defines the working area of the single-point forming tool. The tool is utilized to shape the sheet progressively into a component and its path is generated by a computer numerical control (CNC) machining centre. During the forming process there is no backup die supporting the back surface of the sheet.

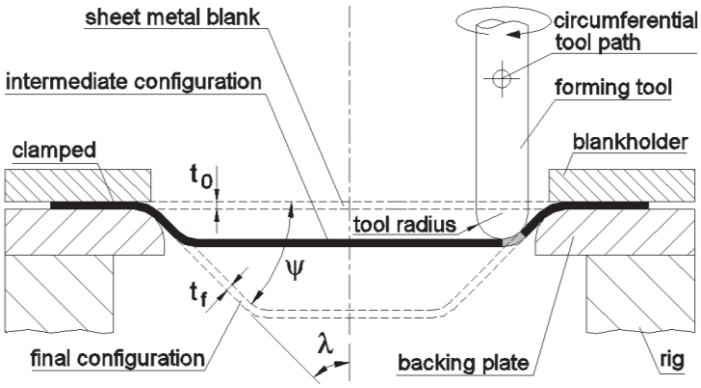

Figure 1. Schematic representation of the SPIF process.

The main advantages of SPIF over conventional sheet-metal-forming processes are:

- the increase in material formability due to the incremental nature of the process;
- the greater flexibility derived from the absence of positive or negative dies;
- the possibility of utilizing conventional CNC milling machines;
- the prospect of easily and quickly evaluating changes in geometry using computer-aided design and computer-aided manufacture (CAM) to produce the parts directly [1].

In the last years the governing mode of deformation in SPIF has been the subject of controversy in the metal-forming community [2]. Some researchers have claimed that deformation takes place by stretching instead of shearing while others have claimed the opposite, but assertions are mainly based on 'similarities' to well-known processes of stamping and shear spinning rather than on experimental evidence from SPIF itself. In previous work [3], the authors presented a theoretical framework built upon the combined utilization of membrane analysis and ductile damage mechanics that is capable of addressing the fundamentals of SPIF of metallic sheets. The theoretical framework accounts for the influence of major process parameters and allows their mutual interaction to be studied both qualitatively and quantitatively. It also allows concluding that the likely mode of material failure in SPIF is consistent with stretching, rather than shearing being the governing mode of

deformation. More recently, numerical simulations combined with the experimental observation of the suppression of necking and the study of the morphology of the cracks enabled the authors to conclude that traditional forming limit curves (FLC's) are inapplicable to describe failure. Instead, fracture forming limit curves (FFLC's) should be employed to evaluate the overall formability of the process [4].

Plastic deformation in SPIF takes place by uniform thinning until fracture without experimental evidence of localized necking before reaching the onset of fracture [3]. The production by SPIF of conventional (i.e. single-stage) parts with shapes having straight vertical walls is impossible since, according to the sine law, a 90º drawing angle would lead to a wall thicknesses equal to zero and strains towards infinity.

This paper deals with new concepts of multistage SPIF that have been recently proposed for eliminating the aforementioned drawback of conventional SPIF related to the production of complex sheet metal parts with vertical walls. The first attempts, as far as the present authors are aware, to utilize multistage SPIF were made by Kitazawa et al. [5] and Kitazawa and Nakane [6] who produced hemi-ellipsoidal axisymmetric parts by employing two sequential stages. The first stage was utilized to shape an intermediate conical geometry that was subsequently formed into the desired hemi-ellipsoidal shape. Later, Kim and Yang [7] and Young and Jeswiet [8] utilized two-stage forming sequences with the purpose of achieving a more uniform distribution of thickness in the parts and concluded that multistage strategies significantly improve the overall formability of the process, allowing the production of parts that could not be obtained by conventional SPIF.

The extension of multistage forming methodologies to variants of incremental sheet metal forming was also attempted by other researchers. For instance, Hirt and co-workers [9, 10] proposed a multistage two-point incremental forming methodology for producing non-axisymmetric sheet metal parts. The approach consists in alternating the tool movement from upwards to downwards and to increase the angle from stage to stage. The number of intermediate stages is chosen to be as small as possible in order to avoid surface wear and to limit the overall forming time. The risk of wrinkling is said to increase with the decrease in the intermediate number of stages.

Very recently Skjoedt et al. [11] and Verbert et al. [12] defined new multistage forming strategies to produce SPIF parts with vertical walls. Skjoedt et al. [11] reported the production of a cylindrical cup, starting from a cone with a 45º angle, and progressively moving the middle of the conical wall towards the corner of the desired cylindrical shape. Verbert et al. [12] presented a cylindrical part that was successfully produced in five steps, starting from a cone angle of 50º and increasing its angle by 10º in each subsequent step. They also showed complex parts produced by means of automatic multistage tool path generation but provided no details on the number of stages and forming sequences. Finally, Duflou et al. [13] studied formability in multistage tool paths and concluded that process windows are extended as a consequence of the straining of (semi)horizontal areas of the parts that remain unaffected in conventional tool path strategies.

The aim of the present paper is threefold: first, to check whether FFLC's can be successfully employed to establish the forming limits of multistage SPIF, second, to discuss the appropriateness of multistage SPIF sequences for fabricating cylindrical cups with vertical

walls and, third, to present three industrial prototypes that were manufactured by the authors using multistage SPIF. The presentation covers both numerical simulation and experimentation research topics. The numerical modelling was performed using the explicit-dynamic finite element computer program LS-DYNA. The experimental work involved material characterization, determination of FLC's and FFLC's, and measurement and calculation of strain paths and fracture strains in SPIF parts.

2. EXPERIMENTAL WORK

The experimental work was performed on aluminium alloy AA1050-O sheet blanks of 1 mm thickness. Tensile and hydraulic bulge tests were utilized for the mechanical and formability characterization of the material. Multistage SPIF experiments were performed in order to fabricate parts with vertical walls and to support the overall numerical and experimental investigation.

2.1. Mechanical characterization and formability limits

The mechanical and formability characterization of the AA1050-O sheet blanks made use of tensile tests and biaxial, circular (diameter, 100 mm), and elliptical (diameters of the major and minor axes, 100 mm and 63 mm respectively) hydraulic bulge tests (Figure 2a). The tensile tests were performed in a universal materials-testing machine (Instron 4507), in accordance with the standard for tensile tests NP EN 10 002-1 [14] and the hydraulic bulge tests were performed in a universal sheet-metal-testing machine (Erichsen 145/60).
The results obtained for the tensile tests are presented in Table 1. The symbol E denotes Young's modulus, σ_Y is the yield strength, A is the uniform elongation at break point, and U_T is the toughness.

Parameter (units)	Value
E (MPa)	70 943
σ_Y (MPa)	119.9
U_T (MPa)	9.33
A (%)	10

Table 1. Results from the tensile tests on AA1050-O sheets.

The stress–strain curve of aluminium alloy AA1050-O derived from the tensile tests is given by,

$$\bar{\sigma} = 153\,\bar{\varepsilon}^{0.25}\ MPa \tag{1}$$

The technique utilized for obtaining the FLC involved electrochemical etching of a grid of circles with 2 mm initial diameter on the surface of the sheets before forming and measuring the major and minor axis of the ellipses that result from the plastic deformation of the circles during the formability tests. The values of strain were computed from (refer to Figure 2b),

$$\varepsilon_1 = \ln\left(\frac{a}{2R}\right) \qquad \varepsilon_2 = \ln\left(\frac{b}{2R}\right) \tag{2}$$

where the symbol R represents the original radius of the circle and the symbols a and b denote the major and minor axis of the ellipse.
The resulting FLC is plotted in Figure 2c and was constructed by taking the principal strains $(\varepsilon_1, \varepsilon_2)$ at failure from grid-elements placed just outside the neck (that is, adjacent to the region of intense localization) since they represent the condition of the uniformly-thinned sheet just before necking occurs [15].
The intersection of the FLC with the major strain axis is found to occur at $\varepsilon_1 = 0.24$ in good agreement with the value of the strain hardening exponent of the stress-strain curve obtained by means of tensile tests, (equation (1)).

(a)

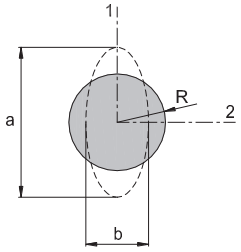

(b)

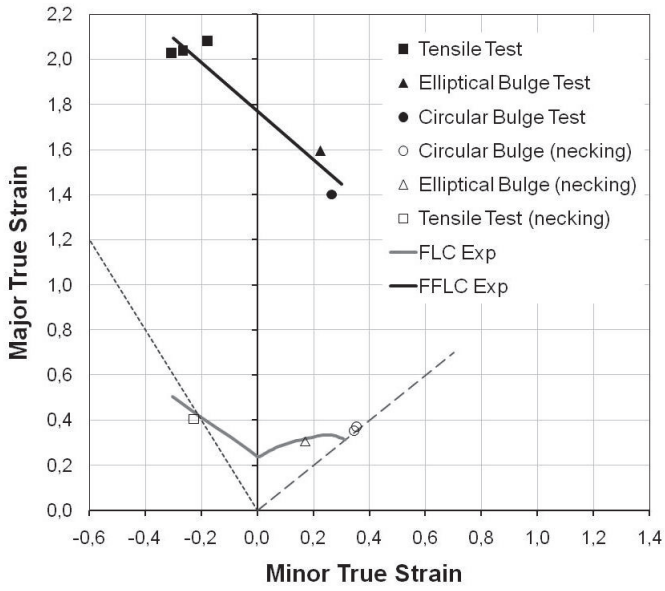

(c)

Figure 2. Experimental determination of the FLC and FFLC for aluminium AA1050-O sheets with 1 mm thickness. (a) Tensile, elliptical and circular hydraulic bulge test specimens, (b) schematic representation of the major and minor axis of the ellipses that result from the plastic deformation of the grids of circles and (c) FLC and FFLC in the principal strain space.

The experimental FFLC is more difficult to obtain than the FLC. Application of grids even with very small circles in order to obtain strains in the necking region after it forms and, therefore, close to the fracture, provides strain values that cannot be considered the fracture strains. Moreover, such grids create measurement problems and suffer from sensitivity to the initial size of the circles due to the inhomogeneous deformation in the neighbourhood of the crack.
As a result of this, the experimental procedure for constructing the FFLC required measuring of thickness before and after fracture at several places along the crack in order to obtain the 'gauge length' strains. The strain in the width direction was obtained differently for tensile and bulge tests. In case of tensile tests measurements were directly taken from the width of

the specimens whereas in case of bulge tests measurements required the utilization of the imprinted grid of circles in order to obtain the initial and deformed reference lengths. The procedures are illustrated in Figure 3.

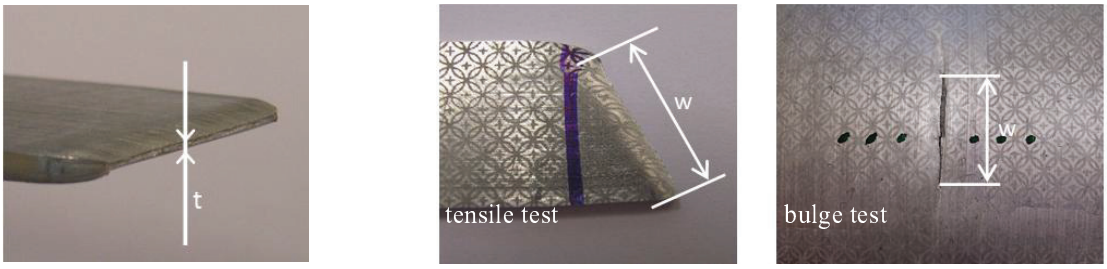

(a) (b)

Figure 3. Experimental procedures that were utilized for obtaining the experimental values of strain along the (a) thickness and the (b) width directions at the onset of fracture.

The third fracture strain component, in the plane of the sheet with direction perpendicular to the crack, was determined by volume constancy knowing the two other strains.
The strains at the onset of fracture are plotted in Figure 2c and the FFLC is approximated by a straight line $\varepsilon_1 + 1.08\varepsilon_2 = 1.77$ falling from left to right in good agreement with the condition of constant thickness strain at fracture (given by a slope of '-1') proposed by Atkins [16].
The large distance between the neck formation FLC and the fracture FFLC in Figure 2c indicates that AA1050-O is a very ductile material allowing a considerable through-thickness strain within the neck, between neck initiation and fracture.

2.2. Multistage SPIF

In previous work, Skjoedt et al. [11] presented an innovative multistage SPIF strategy that enables the production of a cup with a vertical wall by SPIF. The strategy makes use of the four intermediate stages that are schematically plotted in Figure 4 in order to extend deformation to all the material available.

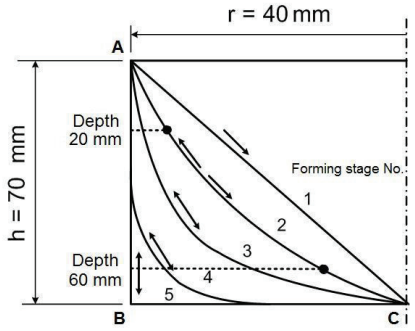

Figure 4. Multistage SPIF strategy for producing a cylindrical cup with vertical walls [9].

The first stage is utilized for forming the sheet blank into a conical shape with a constant

angle of 45º while the subsequent stages are employed for gradually moving the middle of the conical wall towards the corner of the cylinder. All stages, apart from the first, can be performed with the tool moving either downwards or upwards. For convenience, when the movement of the tool is downwards the stage is represented by a D, and when it is upwards by a U.

The fifth stage in Figure 4 is supposed to produce an ideal final shape that is not technologically feasible because it would require the formation of a flat bottom cylindrical cup with a vertical wall and a bottom radius equal to zero. Still, assuming the extreme forming conditions of the fifth stage, the principal strains in the resulting SPIF part can be estimated by considering the deformation to be pure biaxial stretching and the meridional strain ε_ϕ to be evenly distributed. The circumferential strain ε_θ is zero at points A and C and maximum at point B (see Figure 4) and, in the case when $h = r$, the strain field is given by

$$\varepsilon_\phi = \ln\left(\frac{2r}{r}\right) = \ln(2) \qquad \varepsilon_{\theta,\max} = \ln\left(\frac{2\pi r}{\pi r}\right) = \ln(2) \qquad \varepsilon_{t,\max} = -\ln(4) \approx -1.4 \tag{3}$$

Previous investigations by Skjoedt et al. [11, 17] revealed that a multistage SPIF strategy consisting of three downward movements followed by a final upward movement (DDDU) could be successfully employed to produce a sound cylindrical cup with vertical walls. This is the main reason why the overall investigation in the SPIF of cylindrical cups was focused on the analysis of multistage forming strategies that are exclusively based on four intermediate stages.

The tests were performed in a CNC machining centre equipped with an appropriate experimental apparatus. The forming tool has a diameter of 12 mm and a hemispherical tip and was made of cold-work tool steel (120WV4-DIN) hardened and tempered to a Rockwell C hardness of 60 HRC in the working region.

The feed rate was set to 1000 mm/min and the first stage, which has a constant drawing angle, is performed with a vertical step size of 0.5 mm. In subsequent stages it is not advantageous to utilize a fixed vertical step size because it results in a large distance between tool paths in flat regions where the drawing angle is close to zero, e.g. the bottom of the cup. Instead the general distance is set to 1 mm, which results in a vertical step size of 1 mm in sections close to vertical and a vertical step size close to 0 mm in sections which are close to being flat.

Tool paths were generated with the program HeToPaC [18]. The lubricant applied between the forming tool and the sheet was diluted cutting fluid.

The geometries utilized in the intermediate SPIF stages were similar to those plotted in Figure 4, with $h = 70mm$ and $r = 80.5mm$. The initial blanks consisted of square sheets of area 253 mm x 253 mm that were electrochemically etched to imprint a grid with circles of 2 mm diameter on its surface to allow the principal strains to be measured after deformation.

3. FINITE ELEMENT WORK

The finite element model of the sheet blanks were built upon an initial course mesh of 26 x 26 shell elements, each having a side length about 9.7 mm (element type 16 in LS-DYNA). A full integration shell formulation was used with five integration points over the sheet thickness. Adaptive mesh refinement was utilized throughout the computation in order to limit the interference between the sheet and the contours of the forming tool and the backing plate, as well as to obtain high levels of accuracy in terms of geometry and distribution of field variables.

The adaptive mesh refinement procedure consisted of three refinement operations ending up by splitting the original elements into 64 new elements that have one eighth of the initial element size.

The description of the forming tool and of the backing plate was performed by means of surface meshes. Both active tool components were considered rigid and a large number of elements were utilized to model its geometry in order to reduce the level of roughness that was artificially introduced by the overall discretization procedure.

The movement of the tool in the finite element model was identical to that of the actual SPIF process, including the rotation and the helical path, which was defined by means of a large number of points. The number of points was determined by the tolerance setting in the CAM program. Acceleration of the overall central processing unit (CPU) time was performed by means of a load factoring (or time scaling) procedure. This changed the rate of loading by an artificial increase in the velocity of the single-point forming tool by a factor of 1500 for the first stage and a factor of 1000 in subsequent stages, in comparison with the real forming velocity. No mass scaling was used.

The maximum increment of time step for performing the explicit central difference time integration scheme was based on a characteristic length equal to the shell area divided by the longest diagonal. As a precaution, LS-DYNA uses 0.9 times this value to guarantee stability. The material of the sheet was considered isotropic with the stress–strain curve presented in equation (1). No anisotropy effects were taken into consideration.

4. RESULTS AND DISCUSSION

The first part of this section analyses the strain paths resulting from multistage SPIF of cylindrical cups, introduces the forming sequence that allows the production of flat-bottom cylindrical cups with vertical walls and presents a comprehensive discussion on the validity of FFLCs in multistage SPIF. The second part of this section presents three industrial prototypes that were manufactured by the authors using multistage SPIF.

4.1. First stage

Multistage SPIF of cylindrical cups is initiated by producing a cone with a constant drawing angle of 45º in the downward movement of the forming tool. This results in evenly distributed strains along the sheet metal part except close to the backing plate and the bottom region of the cone where the radius is approaching the tool radius. Figure 5(a) presents numerical and experimental values of the major and minor strains over the surface of the parts. The

agreement is very good and the strains are very close to plane strain, as would be expected from conventional SPIF of a conical shape. The finite element computed evolution of the strain paths for two elements of the mesh model located at 10 mm and 60 mm depths at the end of the first stage are close to straight (Figure 5(b)), and the serrated strain paths previously mentioned by other researchers were not observed.
The results also indicate that surface strains are principal strains, meaning that deformation is essentially governed by stretching. If deformation was due to vertical shear or included a large amount of through thickness shear, the surface strains would not be principal strains [4].

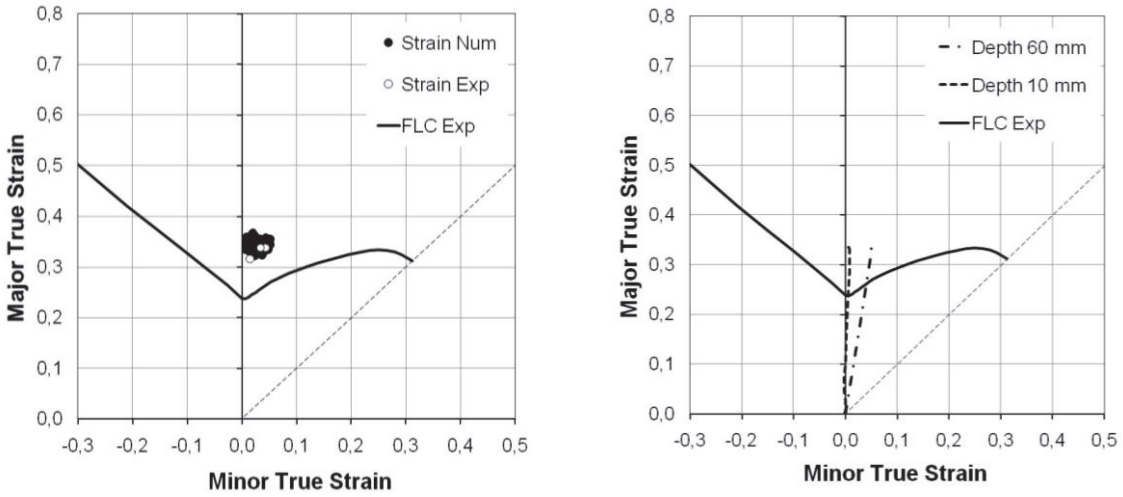

Figure 5. (a) Experimental and numerical strains at the end of the first SPIF stage. (b) The enclosed strain paths are computed from two elements located at 10 and 60 mm of depth.

As seen in Figure 5, the strains at the end of the first stage are already located above the experimental FLC of the aluminium alloy AA1050-O. This is in close agreement with previous claims of the present authors that formability in SPIF is limited by fracture instead of necking [3, 4].

4.2. Second stage

The SPIF part at the end of the second stage can be produced in two different ways: first, DD corresponds to the first as well as the second stage with downward tool movement; second, DU corresponds to the first stage with downward tool movement and the second stage with upward tool movement.
Figures 6a and 6b presents the numerical and experimental values of strain on the surface of the parts for grid locations placed within the depth range 20–60 mm, for the two different tool path combinations. As shown, the DD strategy presents a strain path close to plane strain conditions whereas the DU strategy presents a strain path that is moved towards biaxial strains. The overall agreement between measured and computed values is very good and the results in Figure 6b show that strain paths differ and become highly non-linear in the second

SPIF stage. This seems to be related to the decreasing strain in the ε_1 direction at the beginning of the second stage, corresponding to drawing rather than stretching deformation. The phenomenon is more pronounced in the SPIF parts produced by means of the DU forming strategy.

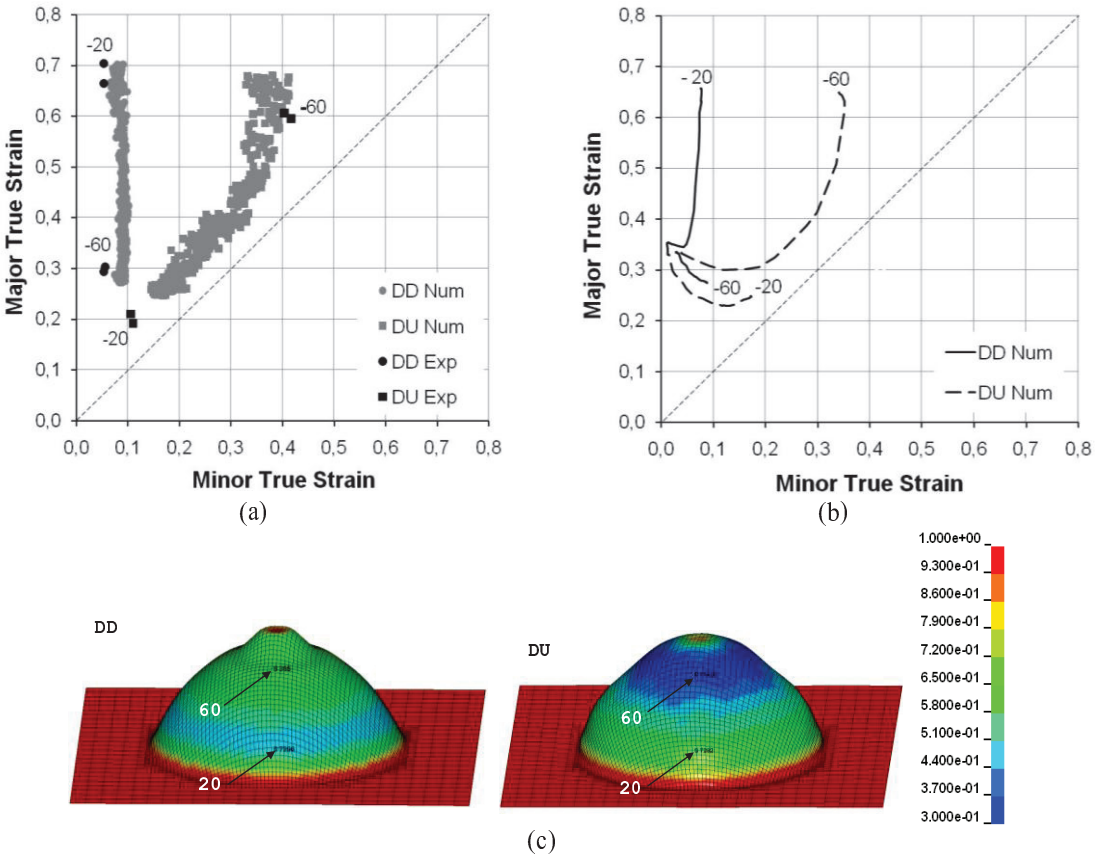

Figure 6. Second SPIF stage. (a) Experimental and numerical strains for DD and DU multistage SPIF strategies. The enclosed strain values are computed within the range of 20 and 60 mm depth. (b) Strain paths computed from two elements located within the range of 20 and 60 mm depth. (c) Numerical distribution of thickness for DD and DU strategies obtained from finite element modelling (scale in mm)

Figure 6c shows the distribution of thickness as a function of depth for DU and DD multistage SPIF strategies obtained from finite element modelling. The DD strategy causes a distribution similar to a conventional single-stage SPIF where increasing angle causes decreasing thickness. Using the DU strategy this is not the case and most of the reduction in thickness occurs in the centre part where the drawing angle is smaller. This is necessary if vertical sides are to be achieved in the subsequent stages.

As seen, the shapes of the two parts differ considerably and, in the case of multistage SPIF with a DD strategy, a residual cone is found to appear at the bottom end of the part. The residual cone is formed because the depth of the part is increased in the second stage, whereas

the tool path only goes down by 70 mm in the first stage. Therefore, as the tool moves downwards during the second stage, a small plateau is formed beneath it (Figure 7(a)). This plateau is observed experimentally as well as in the simulation. The existence of a residual cone has also been reported by Kitazawa and Nakane [6] in their original work on multistage SPIF. In the case of multistage SPIF with a DU strategy, no residual cone is observed after the second stage.

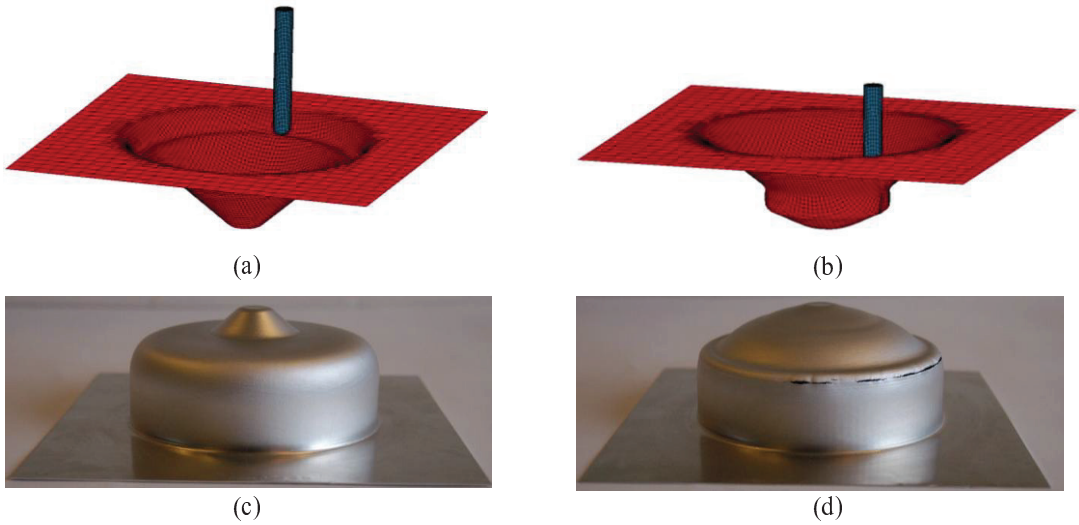

Figure 7. Multistage SPIF of a cylindrical cup. (a) Formation of a plateau during the second stage (DD strategy) obtained from finite element modelling. (b) Formation of a linear contact during the second stage (DU strategy) obtained from finite element modelling. (c) Final part obtained from a multistage DDDU strategy. (d) Final part obtained from a multistage DUD(D) strategy.

However, as shown in Figure 7(b), material builds up in front of the tool and changes the contact condition between the tool and deforming part from point to linear. Again this phenomenon is observed in both experiments and simulations. The linear type of contact causes process forces in the X–Y plane to increase and special care should be taken not to exceed the force limits of the machine when forming harder materials. A similar result was found in the experimental work performed by Kitazawa et al. [5].
However, neither of the aforementioned strategies utilized in the second stage succeeded in the production of flat-bottom cylindrical cups with vertical walls at the end of the multistage SPIF sequence (Figures 7(c) and (d)).

4.2. Multi-stage sequence

The multi-stage SPIF sequence that allows the production of a sound cylindrical cup with vertical walls and a residual cone at the bottom end of the part (Figure 7c) consists of three stages with a downward movement of the tool followed by a fourth stage with an upward movement of the tool (DDDU).
Figure 8 shows the results obtained from experimentation and finite element analysis, and special emphasis is placed on the residual cone that develops immediately after the second

stage and remains until the end of deformation. The overall agreement between experimentation and simulation is good during the first three initial stages but rather poor in the last stage. A possible explanation for this result is the too coarse mesh which is due to a large increase in surface area.

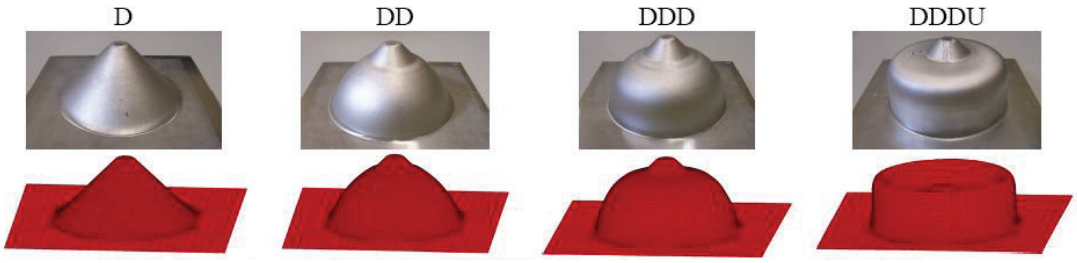

Figure 8. Comparison between experimentation and simulation for each stage in the DDDU strategy.

The elimination of the aforementioned residual cone required enhancement of the multistage SPIF sequence with the aim of producing flat-bottom cylindrical cups with vertical walls (Figure 9).

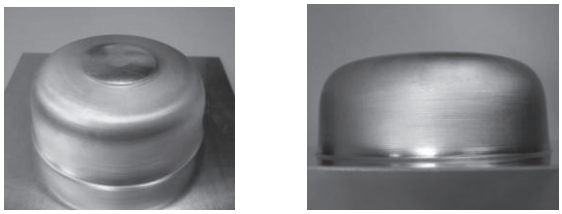

Figure 9. Cylindrical cup obtained by means of the enhanced multistage SPIF strategy.

The enhanced multistage SPIF strategy proposed by the authors makes use of the same number of stages and the same sequence as the previous DDDU strategy shown in Figure 8. The shape resulting from the first stage is the same as the first step of the multi-stage SPIF strategy shown in Figure 8. The second stage produces a deeper shape (55mm) with a radius of curvature $R = 10mm$ at the bottom of the part in order to smooth the transition between the bottom and the conical wall. The third stage is designed to obtain a depth of 65.5mm and the tool is forced to stop when it reaches the flat region located at the bottom centre of the part. The fourth stage is performed by upward movement of the tool starting at the bottom flat centre of the part located at a depth of 66.5mm. Table 2 provides the details.

Stage	Depth (mm)
1 (D)	45
2 (D)	55
3 (D)	65.5
4 (U)	66.5

Table 2. The depths of each stage that were utilized in the enhanced multistage SPIF strategy.

4.3. Formability limits

Table 3 summarizes the multistage SPIF strategies that were analysed in the investigation. The forming stages, where cracking occurred, are indicated in parentheses and the experimental values of fracture strains were always measured for the forming stages that could not be completed because of fracture. The fracture strains were measured using the circle grid technique because no necking was found to occur (see section 2.1).

Strategy	
#1	DDD(D)
#2	DDDU
#3	DUD(D)
#4	DUD(U)
#5	--(D)-

Table 3. The different multi-stage SPIF strategies that were investigated.

It is worth noting that strategy #5 results from the attempt to shape the geometry of the third stage directly from the initial sheet blank without resorting to intermediate forming stages.
The occurrence of fracture in other multi-stage SPIF strategies than DDDU can be easily understood in the principal strain space (Figure 10). This figure contains two different FFLC's: (i) the thick solid line ($\varepsilon_1 + 1.08\varepsilon_2 = 1.77$) is obtained from the fracture strains measured in the experimental tensile and biaxial hydraulic bulge tests (see section 2) while (ii) the dashed line is derived from the critical value of damage at the onset of cracking, and its slope is determined in accordance with previous work published by the present authors [3, 4], according to,

$$\frac{\varepsilon_1^{biaxial} - \varepsilon_1^{planestrain}}{\varepsilon_2^{biaxial} - \varepsilon_2^{planestrain}} = \frac{\Delta\varepsilon_1}{\Delta\varepsilon_2} = -\frac{5(r_{tool}/t)+2}{3(r_{tool}/t)+6} \tag{4}$$

To determine the equation for the dashed line a truncated conical shape characterized by various drawing angles with depth was formed until fracture. The experimental value of the drawing angle at fracture is 77.5º, corresponding to a strain $\varepsilon_1 = 1.5$ and to a final thickness $t = 0.22mm$. By substituting the thickness and the radius of the tool ($r_{tool} = 6mm$) in equation (4) and by taking into account the above-mentioned value of strain at fracture, the corresponding FFLC is given by $\varepsilon_1 + 1.58\varepsilon_2 = 1.5$.
The numerical and experimental values of strain resulting from the entire set of multi-stage SPIF strategies (Table 3) are also plotted in the principal strain space (Figure 10). The values of strains without fracture were measured as well as simulated in the first three stages (DDD and DUD) and only measured in the fourth stage. As seen, all the strain points corresponding to sound SPIF conditions (DDD, DUD and DDDU plotted as open marks) are located below the FFLC's. Moreover, the agreement between FFLCs and fracture points (DDD(D), DUD(U) and DUD(D) plotted as solid marks) is also good. Major deviations are found in the comparisons with the experimental FFLC and can be attributed to the measuring procedure of the gauge length strains because it is difficult to execute whenever the thickness of the

specimens is very small. This is the reason why a 15 per cent uncertainty interval is recommended to be plotted around the experimentally determined FFLC (see the grey area in Figure 10).

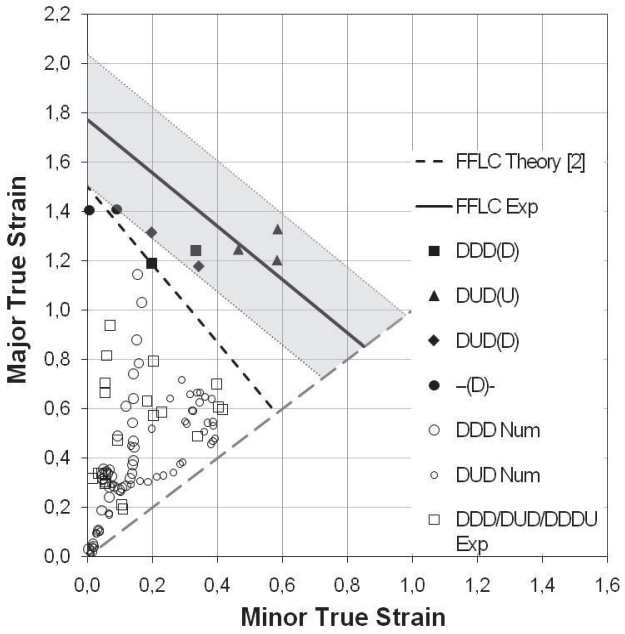

Figure 10. Fracture forming limit diagram containing the FFL's and the strain values obtained for different multistage SPIF strategies.

The difference between the two FFLC's can also be explained by the fact that the experimental data (solid line) provides a general fracture line constructed from different testing methods (i.e. bulge and tensile tests) whereas the theoretical FFLC (dashed line) is built upon an analytical framework that was specifically developed for SPIF and a strain point $(\varepsilon_1, \varepsilon_2)$ at failure that needs to be obtained from SPIF experiments [3]. The three failure points for the DUD(U) strategy seem to be outliers and this can be a result of the linear contact between tool and workpiece which is observed as the tool moves upwards (see section 4.2). In fact, the theoretical FFLC is derived under the assumption of a small contact area localized at the radius of the tool instead of a linear contact along the side of the tool.

5. INDUSTRIAL APPLICATIONS

This section of the paper presents three examples of industrial prototypes that were produced by means of multistage SPIF. The first prototype is a sector shower tray made from aluminium AA1050-O and its fabrication process will be comprehensively described. The second and third prototypes were made from steel and polycarbonate for the home appliance and automotive industries.

Sector shower tray

Producing a sector shower tray by multistage SPIF offers the challenge of manufacturing a sheet metal prototype with vertical walls (Figure 11) that goes in-line with the fundamental research work that was presented in the previous sections of the manuscript.

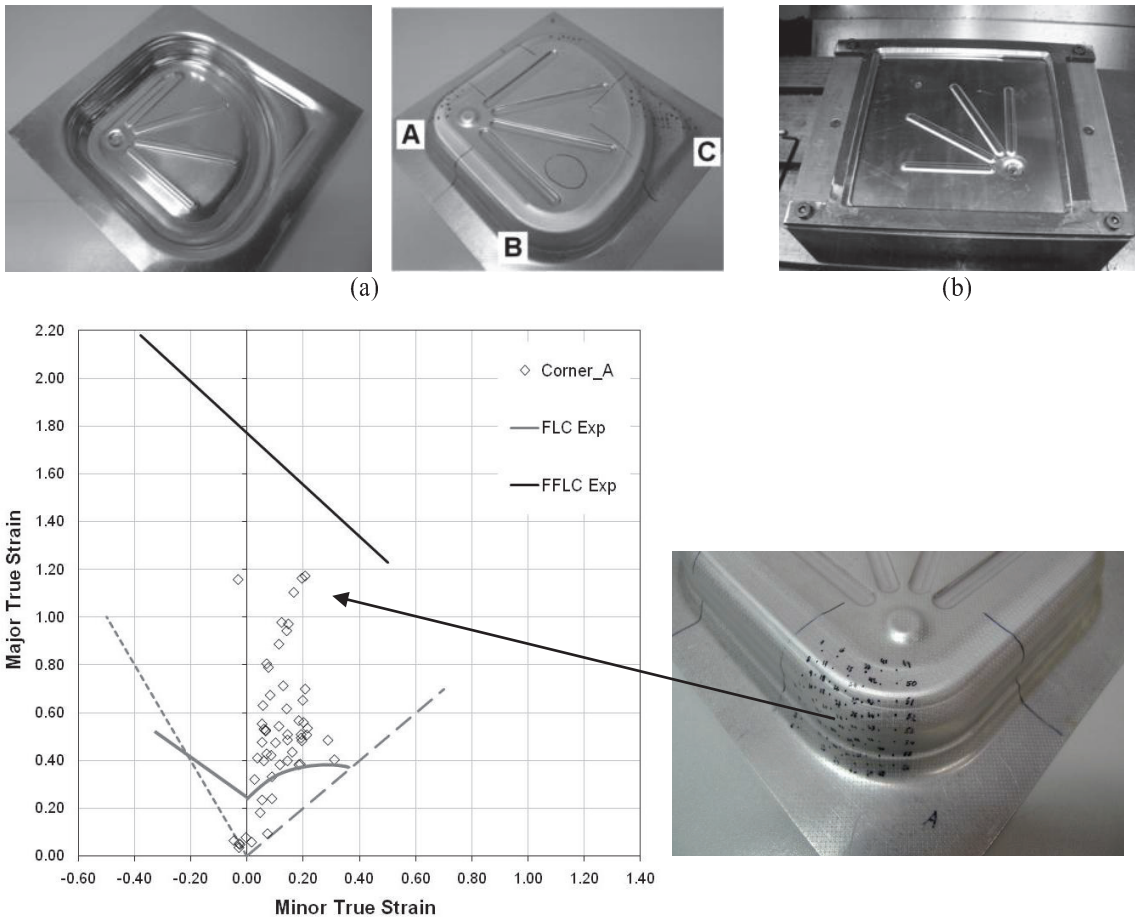

Figure 11. SPIF of a sector shower tray (250 x 250 mm, scale 1:1). (a) Final part showing the circle grids that were utilized for measuring the strains at the bottom side of the part, (b) prototype at the end of the first stage and (c) principal strain space containing the results from circle grid analysis for the corner of the sector shower tray labelled 'A'.

The sector shower tray was produced in six different stages. The first stage was utilized to produce the stripes and the circular depression shown in Figure 11b while the subsequent stages, to be performed after turning over the sheet, were employed to obtain the top area (2nd stage) and to gradually form the vertical walls (3rd to 6th stages).
The results from circle grid analysis for the most critical corner of the sector shower tray (labelled 'A' in Figure 11a, are shown in Figure 11c. Strains are located well above the experimental FLC but beneath the FFLC, in close agreement with the formability limits of the

Aluminium AA1050-O that were experimentally determined by means of tensile tests and circular and elliptical bulge tests (refer to section 2.1).

Component for a microwave oven

The second prototype is a component for microwave oven made from stainless steel AISI 430 with 0.5 mm of thickness. The original geometry and the corresponding prototype fabricated by multistage SPIF are shown in Figure 12.

(a) (b)

Figure 12. SPIF of a microwave oven component (400 x 300 mm, scale 1:3). (a) Geometry and (b) prototype.

The microwave oven component was produced in two different stages followed by cutting and bending of the sides. The first stage is utilized to produce the rectangular frame and the top prismatic depression (Figure 13a) while the second stage, to be performed after turning over the sheet, was employed to form the central rectangular area (see Figure 13b).

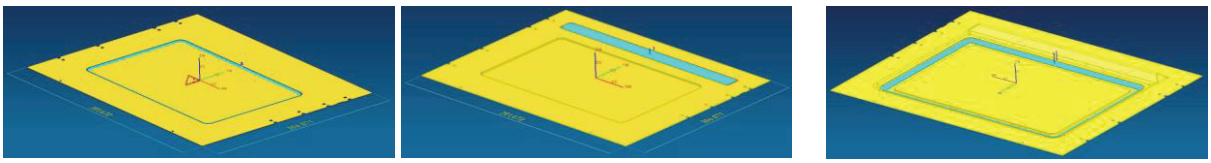

(a) (b)

Figure 13. Forming strategies in the multistage SPIF of a microwave oven component, (a) first stage and (b) second stage.

Because the prototype produced by SPIF revealed a considerable springback after being formed (refer to Figure 12b) it was decided to redesign the part in order to include two additional cross stripes. This modification of the original geometry revealed successful in diminishing the overall springback.

In addition to the work performed in stainless steel, authors were also able to manufacture a polycarbonate component with 2 mm of thickness using the same multistage forming sequence (Figure 14). The component made from polycarbonate revealed interesting for equipment showrooms because polycarbonate keeps transparency after being formed by SPIF (Figure 14).

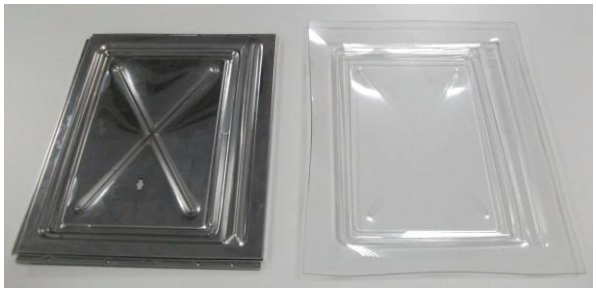

Figure 14. Redesigned SPIF components made from stainless steel and polycarbonate.

Upper seat-back frame of an automotive

The third prototype is an upper seat-back frame of an automotive made from DC04 steel with 0.6 mm of thickness. The original drawing, the prototype produced by SPIF and the industrial part fabricated (in mass production) by conventional stamping are shown in Figure 15.

(a) (b) (c)

Figure 15. Upper seat-back frame of an automotive (580 x 450 mm, scale 1:1). (a) Drawing, (b) prototype fabricated by SPIF and (c) industrial component fabricated by conventional stamping.

The prototype of the upper seat-back frame was produced in two stages (Figure 16). The first stage is utilized for shaping the inner stripes and the second stage, to be performed after turning over the sheet, was employed to form the central depression.

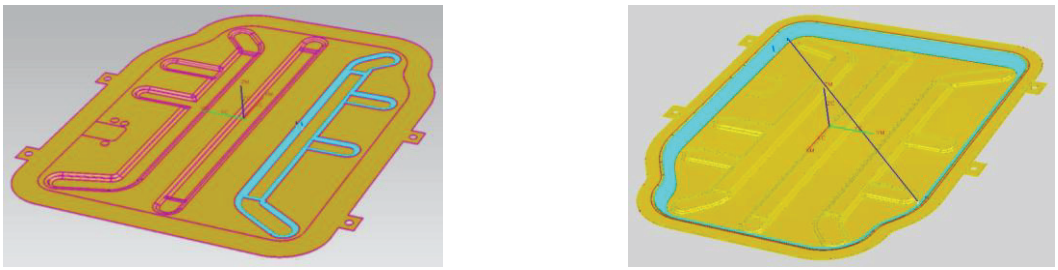

(a) (b)

Figure 16. Multistage forming sequence for producing the upper seat-back frame of an automotive by SPIF. (a) first stage and (b) second stage.

6. CONCLUSIONS

Multistage SPIF allows rapid prototyping of complex geometries with vertical walls. The movement of the tool (upwards or downwards) in multistage SPIF has a considerable effect on the thickness distribution and position of strain points in the principal strain space. Tool paths going upwards imply more biaxial strains than downward tool paths, which are closer to plane strain conditions. The strain paths are linear in the first stage and highly non-linear in the subsequent stages.

The FFLC independently determined from tensile and hydraulic bulge tests can be successfully utilized for establishing the formability limits of multi-stage SPIF provided that an uncertainty interval is taken into consideration in order to avoid errors attributed to the measurement of the gauge length strains. The correlation between the experimental FFLC and that resulting from the theoretical framework proposed by the present authors [3, 4] is good and supports the claim that SPIF is limited by fracture instead of necking. In fact, the overall level of strains achieved in multi-stage SPIF is much higher than the experimental values of necking currently found in conventional sheet metal forming.

The industrial examples included in the presentation illustrate the feasibility of multistage SPIF for producing small batches and prototypes with significant savings in both material and energy requirements when compared to conventional stamping. The extension of multistage SPIF to polymers seems to be feasible as shown in the prototype made from polycarbonate.

ACKNOWLEDGEMENTS

The authors would like to thank MSc. João Câmara, Tomas Ladecky and Peter Soe Nielsen.
Maria Beatriz Silva and Paulo Martins would like to thank the opportunity and support provided by MCG - Mind for Metal, Carregado, Portugal and Fundação para a Ciência e a Tecnologia, Ministério da Ciência, Tecnologia e Ensino Superior, Portugal (Project PTDC/EME-TME/098728/2008).

REFERENCES

[1] J. Jeswiet, F. Micari, G. Hirt, A. Bramley, J. Duflou, and J. Allwood, “Asymmetric single point incremental forming of sheet metal”, *CIRP Ann. –Mfg Technol.* Vol. **54**, pp. 623–650, (2005).

[2] W.C. Emmens and A.H. van den Boogaard, “Strain in shear and material behaviour in incremental forming”, *Key Engineering Materials* Vol. **344**, pp. 519-526, (2007).

[3] M.B. Silva, M. Skjoedt, A.G. Atkins, N. Bay and P.A.F. Martins, “Single-point incremental Forming and formability-failure diagrams”, *The Journal of Strain Analysis for Engineering Design* Vol. **43**, pp. 15-35, (2008).

[4] M.B. Silva, M. Skjoedt, N. Bay and P.A.F. Martins, “Revisiting single point incremental forming & formability/failure diagrams by means of finite elements and experimentation”, The Journal of Strain Analysis for Engineering Design Vol. **44**(4), pp. 221-234, (2009).

[5] K. Kitazawa, A. Wakabayashi, K. Murata and K. Yaejima, “Metal-flow phenomena in computerized numerically controlled incremental stretch-expanding of aluminium

sheets", *Journal of Japan Institute of Light Metals* Vol. **46**, pp. 65-70, (1996). (in Japanese)

[6] K. Kitazawa and M. Nakane, "Hemi-ellipsoidal stretch expanding of aluminum sheet by CNC incremental forming process with two path method", J*ournal of Japan Institute of Light Metals* Vol. **47**, pp. 440-445, (1997). (in Japanese)

[7] T.J. Kim and D.Y. Yang, "Improvement of formability for the incremental sheet metal forming process", *International Journal of Mechanical Sciences* Vol. **42**, pp. 1271-1286, (2000).

[8] D. Young and J. Jeswiet, "Wall Thickness Variations in single Point Incremental Forming", *Journal of Engineering Manufacture* Vol. **217**, pp. 1571-1581, (2003).

[9] G. Hirt, J. Ames, M. Bambach and R. Kopp, "Forming strategies and Process Modeling for CNC Incremental Sheet Forming", *Annals of CIRP* Vol. **52**(1), pp. 203-206, (2004).

[10] M. Bambach, G. Hirt and J. Ames, *Modeling of Optimization Strategies in the Incremental CNC Sheet Metal Forming Process*. *Numiform 2004 – Proceedings of the 8th International Conference on Numerical Methods in Industrial Forming Processes*, Columbus, Ohio, (2004), pp. 1969-1974.

[11] M. Skjoedt, N. Bay, B. Endelt and G. Ingarao, *Multi Stage Strategies for Single Point Incremental Forming of a Cup. 11th ESAFORM 2008 Conference on Material Forming*, Lyon, France, (2008).

[12] J. Verbert, B. Belkassem, C. Henrard, A.M. Habraken, J. Gu, H. Sol, B. Lauwers and J.R. Duflou, *Multi-Step toolpath approach to overcome forming limitations in single point incremental forming. 11th ESAFORM 2008 Conference on Material Forming*, Lyon, France, (2008).

[13] J.R. Duflou, J. Verbert, B. Belkassem, J. Gu, H. Sol, C. Henrard and A.M. Habraken, "Process window enhancement for single point incremental forming through multi-step toolpaths". *CIRP Ann. –Mfg Technol.* Vol. **57**, pp. 253–256, (2008).

[14] NP EN 10002-1 – *Metallic materials: Tensile testing. Part 1: Method of test (at room temperature)*, (1990) (Instituto Português da Qualidade, Caparica).

[15] C. Rossard, *Mise en forme des métaux et alliages*, Centre National de la Recherche Scientifique – CNRS, Paris, (1976). (in French)

[16] A.G. Atkins, *Fracture mechanics and metal forming: damage mechanics and the local approach of yesterday and today* in Fracture Research in Retrospect (ed. H. P. Rossmanith), A.A. Balkema, Rotterdam, pp. 327-350, (1997).

[17] M. Skjoedt, M.B. Silva, P.A.F. Martins and N. Bay, *Strain paths and fracture in multi stage single point incremental forming. ICTP-2008, 9th International Conference on Technology of Plasticity*, Gyeongju, Korea, (2008).

[18] M. Skjoedt, M.H. Hancock and N. Bay, "Creating helical tool paths for single point incremental forming", *Key Engineering Materials* Vol. *334*, pp. 583-590, (2007).